AIAA JOURNAL
Vol. 42, No. 6, June 2004

Finite Element Interface Technology for Modeling Delamination Growth in Composite Structures

Antonio Pantano* and Ronald C. Averill†
Michigan State University, East Lansing, Michigan 48824-1226

An effective and robust interface element technology is presented for connecting and simulating crack growth between independently modeled finite element subdomains, for example, composite plies. This method has been developed using penalty constraints and allows coupling of finite element models whose nodes do not necessarily coincide along their common interface. Additionally, the present formulation leads to a computational approach that is very efficient and completely compatible with existing commercial software. The present interface element has been implemented in the commercial finite element code ABAQUS as a user element subroutine, making it easy to test the approach for a wide range of problems. Additionally, the interface element formulation has been modified to simulate delamination growth in composite laminates. Thanks to its special features, the interface element approach makes it possible to release portions of the interface surface whose length is smaller than that of the finite elements. In addition, the penalty parameter can vary within the interface element, allowing the damage model to be applied to a desired fraction of the interface between the two meshes. Results for double cantilever beam and end-loaded split specimens are presented. These results are compared to measured data to assess the ability of the present damage model to simulate delamination growth.

Introduction

WITH model sharing and large-scale analysis activities on the rise, it is becoming evident that improved technology for building computer models is needed. One issue that arises often is the need to perform a unified analysis of a structural assembly using substructural models created independently. These substructural models are frequently created by different engineers using different software and in different geographical locations, with little or no communication between the teams of engineers creating the models. As a result, these models are likely to be incompatible at their interfaces, which makes it very difficult to combine them for a unified analysis of the entire assembly. Finite element interface technology has been developed during the past decade to facilitate the joining of independently modeled substructures.

Unconventional approaches have been employed to connect special elements based on analytical solutions to finite element models.[1,2] To take advantage of parallel computing, Farhat and Roux[3] and Farhat and Gerardin[4] developed a domain decomposition approach. In another work,[5] nonconforming "mortar" elements are employed to connect incompatible subdomains. The finite element interface technology developed at NASA Langley Research Center[6–10] and elsewhere[11] allows the connection of independently modeled substructures with incompatible discretization along the common boundary. This approach has matured to a point that it is now very effective. However, because the interface technology utilizes Lagrange multipliers to enforce the interface constraint conditions, the resulting system of equations is not positive-definite. Recently, an alternative formulation for the finite element interface technology based on Lagrange multipliers has been developed.[12] The alternative approach recasts the interface element constraint equations in the form of multipoint constraints. This change allows an easier implementation of the formulation in a standard finite element code and alleviates the issues related to the resulting nonpositive-definite system of equations. The method seems to provide reliable results, but the formulation of the interface method is still quite complicated.

A possible remedy for these shortcomings is to modify the current hybrid variational formulation of the interface element by enforcing the interface constraints via a penalty method as opposed to the current Lagrange multiplier approach. The primary consequences of this modification will be 1) a simple formulation that is easily implemented in commercial finite elements codes, 2) a positive-definite and banded stiffness matrix, and 3) a reduced number of degrees of freedom (DOF) because the Lagrange multiplier DOF will not be present. Thus, the penalty approach should greatly enhance the computational efficiency of the interface element technology.

From an accuracy point of view, the penalty method enforces the constraints only approximately, depending on the value of the penalty parameter chosen, whereas the Lagrange multiplier approach enforces the constraints exactly. The penalty method interface approach was recently attempted using a single global value of the penalty parameter to enforce all constraints.[13] This study demonstrated the validity and the effectiveness of the penalty approach in an interface element. However, there is need for specific guidelines regarding the selection of an appropriate value of the penalty parameter, especially when the substructures to be connected have different material and/or section stiffnesses. A criterion for choosing the penalty parameter in the framework of the interface element under investigation has been developed by the authors, as described subsequently. This paper will review the penalty-based interface element technology and subsequently introduce a new application of the interface element for predicting delamination crack growth in laminated structures.

General Description of the Interface Element

Consider two independently modeled subdomains Ω_1 and Ω_2 as shown in Fig. 1 for a two-dimensional geometry. The two substructures are connected to each other using an interface element acting like glue at the common interface.

The interface element is discretized with a set of nodes that are independent of the nodes at the interface in the subdomains Ω_1 and Ω_2. The coupling terms associated to the interface element are arranged in the form of a stiffness matrix and assembled with the other finite element stiffness matrices as usual.

The nodal displacements of the subdomain Ω_j are identified by q_j^0 and q_j^i. The superscript 0 marks the DOF that are not on the

Received 9 October 2002; revision received 12 January 2004; accepted for publication 28 January 2004.

*Postdoctoral Associate, Department of Mechanical Engineering. Member AIAA.

†Associate Professor, Department of Mechanical Engineering, 2555 Engineering Building; averillr@egr.msu.edu.

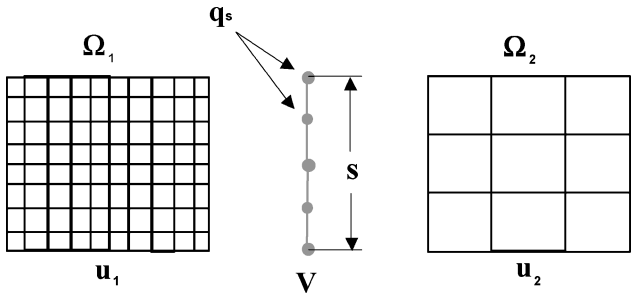

Fig. 1 Connection of an incompatible two-dimensional mesh using interface elements.

interfaces, whereas i denotes DOF that are on the interfaces. The displacement field u_j of the subdomain $\mathbf{\Omega}_j$ is expressed in terms of the unknown nodal displacements q_j^i. The displacement field V is approximated on the entire interface surface in terms of unknown nodal displacements q_s:

$$u_j = N_j\, q_j^i, \qquad V = T\, q_s \tag{1}$$

where N_j can be the matrices of linear Lagrange interpolation functions and T is a matrix of cubic spline interpolation functions. In the penalty interface method, the displacement continuity constraint is imposed in a least-squares sense through two vectors of penalty parameters γ_1 and γ_2. Thus, the total potential energy of the system assumes the form

$$\pi = \pi_{\Omega_1} + \pi_{\Omega_2} + \frac{\gamma_1}{2}\int_S (V - u_1)^2\, \mathrm{d}s + \frac{\gamma_2}{2}\int_S (V - u_2)^2\, \mathrm{d}s \tag{2}$$

The first variation of π is taken with respect to all of the DOF, but not the vectors of penalty parameters γ_1 and γ_2, which are predetermined constants:

$$\delta\pi\,|_{q_1^0, q_1^i, q_S, q_2^0, q_2^i} = 0 \tag{3}$$

The global system of equations of the penalty hybrid interface method assumes the following form:

$$\begin{bmatrix} K_1^{00} & K_1^{0i} & 0 & 0 & 0 \\ K_1^{i0} & K_1^{ii} + G_1^{ii} & -G_1^{is} & 0 & 0 \\ 0 & -G_1^{si} & G_1^{ss} + G_2^{ss} & -G_2^{si} & 0 \\ 0 & 0 & -G_2^{is} & K_2^{ii} + G_2^{ii} & K_2^{i0} \\ 0 & 0 & 0 & K_2^{0i} & K_2^{00} \end{bmatrix} \begin{Bmatrix} q_1^0 \\ q_1^i \\ q_s \\ q_2^i \\ q_2^0 \end{Bmatrix} = \begin{Bmatrix} f_1^0 \\ f_1^i \\ 0 \\ f_2^i \\ f_2^0 \end{Bmatrix} \tag{4}$$

where

$$G_j^{ii} = \gamma_j \int_S \left(N_j^T\, N_j\right) \mathrm{d}s, \qquad G_j^{is} = \gamma_j \int_S \left(N_j^T\, T_j\right) \mathrm{d}s$$

$$G_j^{si} = \left[G_j^{is}\right]^T, \qquad G_j^{ss} = \gamma_j \int_S \left(T_j^T\, T_j\right) \mathrm{d}s \tag{5}$$

This is a symmetric, banded, and positive definite (after boundary conditions are imposed) global stiffness matrix. The stiffness matrix and generalized vector of unknown displacements associated with the interface element can be defined as

$$\begin{bmatrix} G_1^{ii} & -G_1^{is} & 0 \\ -G_1^{si} & G_1^{ss} + G_2^{ss} & -G_2^{si} \\ 0 & -G_2^{is} & G_2^{ii} \end{bmatrix} \begin{Bmatrix} q_1^i \\ q_s \\ q_2^i \end{Bmatrix} = \begin{Bmatrix} 0 \\ 0 \\ 0 \end{Bmatrix} \tag{6}$$

Determination of the Penalty Parameters

In the penalty method, the displacement continuity constraint is imposed through penalty parameters, a set of predetermined constants. The finite element (FE) solution obtained using this method is approximate, with its accuracy depending on the value of the adopted penalty parameters. It is known that the penalty parameter should depend on the material and/or geometric properties of the two subregions being joined. Furthermore, there is a relationship between the penalty parameter and the Lagrange multiplier that enforces a given constraint. The Lagrange multiplier method imposes the continuity constraint exactly; thus, it defines the upper limit to the accuracy of the penalty method. Knowledge of the correct solution facilitates relating the value of the penalty parameter to the geometrical and material properties of the model under consideration. In our pursuit of the proper penalty parameter values, a variety of one- and two-dimensional problems have been studied with both the Lagrange multiplier method and the penalty method. The types of finite elements that have been investigated are conventionally formulated and reduced integrated Timoshenko beam elements, plane stress quadrilateral elements, and plate elements based on the first order shear deformation theory (FSDT), or Mindlin plate theory. For each FE formulation, different penalty parameters are associated to the various nodal DOF. For example, the Timoshenko beam element has three independent nodal DOF: the axial displacement u, the transverse displacement w, and the rotation ψ. Thus, three different penalty parameters, γ_u, γ_w, and γ_ψ, are employed to enforce the interface continuity constraints on the DOF u, w, and ψ. An independent choice of the penalty parameters is necessary because each DOF can be related differently to the material and geometric properties of the FE model.

The methodology adopted in finding the relations will now be described. First the most common load cases for the FE type under consideration are applied separately to a simple model of one or two elements. The formulations and solutions are obtained using both the Lagrange multiplier method and the penalty method. The displacement solutions from the two methods are compared individually for each DOF. The ratio between the two solutions is expressed in the form

$$u^{\text{penalty}} \big/ u^{\text{Lagrange}} = 1 + f/\gamma \tag{7}$$

where $f = f$ (element geometric properties, material properties, and loads).

Once this simple expression has been identified, the penalty parameter γ is set equal to $\gamma = \beta f$. Then, the ratio between the solutions becomes independent of material and geometrical properties:

$$u^{\text{penalty}} \big/ u^{\text{Lagrange}} = 1 + 1/\beta \tag{8}$$

The accuracy of the solution depends directly on the value assigned to the parameter β. The degree of precision of the solution cannot be indefinitely increased, because roundoff amplification error would rise. However, once a reasonable compromise between constraint representation error and the roundoff error has been evaluated, a value of β can be identified that is able to produce the same level of accuracy for every combination of material and geometrical properties.

The present model has been applied only in implicit analyses. For explicit analyses, a very high penalty parameter may have a negative impact on the stable time step. Fortunately, it has been found that low values of β can often be used successfully to connect two subregions.

Interface Technology for Modeling Delamination

The interface element developed in the present study can be readily employed for the analysis of delamination growth in composite laminates. In addition, the present interface element approach would have several advantages over the conventional FE one. A special feature, which is useful in simulating delamination, is the ability of releasing desired portions of the interface smaller than the FE length, determining the crack advance. This can be achieved by changing the extreme values of the interval of integration of the interface element or by reducing the value of the penalty parameter for that interval. Also, within each interface subregion, it is possible to evaluate forces at the interface and to reduce the value of the penalty parameter as needed. Thus, it is possible to overcome the limitation common to the delamination techniques found in the literature, which requires delamination growth to be simulated in a discretized form by releasing nodes of the FE model.

The damage model currently implemented in the developed interface element is one that is commonly adopted.[14–21] It mixes features of strength of materials approaches and fracture mechanics. A bilinear softening model has been implemented in the present model, which assumes an initial linear elastic range up to the point of initial crack formation, followed by a linear decrease in stress carrying capability as the crack continues to open (Fig. 2). In single-mode delamination, as the load is progressively increased, the relative displacement δ between the bottom and top FE mesh grows proportionally according to the value of the penalty stiffness γ. When δ_0 is reached, the stress is equal to the interfacial tensile strength σ_t, the maximum stress level possible. For higher relative displacements, the interface accumulates damage and its ability to sustain stress decreases progressively. Once δ exceeds δ_F, the interface is fully debonded and it is no longer able to support any stress. If the load were removed after δ_0 has been exceeded but before δ_F has been reached, the model would unload to the origin. For example, if after reaching point K the load is reduced, the model unloads along the line KO (Fig. 2). If the load is reapplied, the stress grows with the relative displacement along the same line KO.

This behavior is obtained by an effective reduction in the penalty stiffness γ. In the present model, a new parameter D is introduced to signify the damage accumulated at the interface:

$$\sigma = (1 - D)\gamma\delta \tag{9}$$

Thus, D is a damage parameter, whose initial value is zero. D starts growing when $\delta \geq \delta_0$ and reaches the value 1 when $\delta \geq \delta_F$.

The value of D is computed from geometry to be

$$D(\delta) = \frac{\delta_F(\delta - \delta_0)}{\delta(\delta_F - \delta_0)} \tag{10}$$

The interfacial constitutive model is entirely defined when two of the following properties are known: G_c, σ_t, δ_0, and δ_F. The following two relations exist among these parameters:

$$G_c = \delta_F\sigma_t/2 \tag{11}$$

$$\delta_0 = \sigma_t/\gamma \tag{12}$$

The bilinear interface model is applied to a subregion of the interface between the two meshes; the smaller is the length of each subregion, the higher is the accuracy of the prediction. A conventional implementation of the discussed damage technique requires the model to be applied along the length of one FE, wherein the crack can advance in a discrete way only by failing one element at a time. Both limitations necessitate the use of a refined FE mesh. Thanks to the special features of the interface element presented earlier, the damage evolution scheme in our model is effectively mesh independent, wherein subregions of the interface much smaller than the FE length can be released.

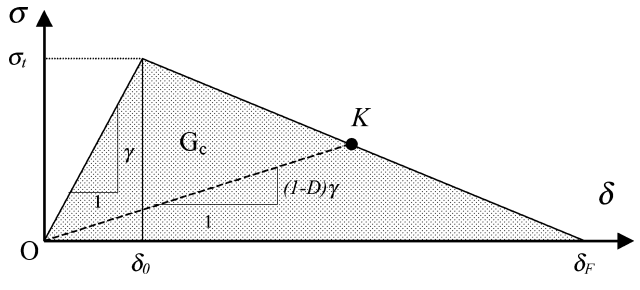

Fig. 2 Bilinear interfacial constitutive damage model.

Thus, the bilinear interface model can be applied to a desired fraction of the interface between the two meshes. If we divide the interface element into a given number of intervals n, each of them will obey the rules of the failure model independently from the others. This corresponds to changing the total potential energy of the system in the following way:

$$\pi = \pi_{\Omega_1} + \pi_{\Omega_2} + \frac{1}{2}\sum_{i=1}^{n}(1 - D_i)\gamma_1\int_{L_{i-1}}^{L_i}(V - u_1)^2\,\mathrm{d}s + \sum_{i=1}^{n}(1 - D_i)\gamma_2\int_{L_{i-1}}^{L_i}(V - u_2)^2\,\mathrm{d}s \tag{13}$$

where D_i is the damage parameter associated with the interval i and the interval i is defined over the range (L_{i-1}, L_i). L_i is the value of the interface coordinate L at the end of the ith interval. The value of the relative displacement δ is evaluated at the center of the interval i. When the crack is allowed to advance in a more continuous way, a higher accuracy of the simulation can be achieved.

To illustrate this concept, consider the two incompatible meshes shown in Fig. 3. They are joined by two interface elements whose length equals that of five conventional elements of the top mesh and four elements of the bottom mesh. Two forces F applied at the tip are responsible for affecting a mode 1 stress field at the interface. The interface element at the crack tip is shown in Fig. 3a as divided in 10 intervals. The intervals do not need to match any of the nodes in the upper or lower mesh, but in this example some of them coincide. Moreover, the number of intervals in the interface element is a parameter that can be changed as desired. Following the progression in Fig. 3, a simulation of the delamination growth is achieved by releasing portions (intervals) of the interface element. In Fig. 3b, the first interval is failed. The portion of the interface element not released still applies its constraint to the lower and upper element next to the crack tip.

In Fig. 3c, the second interval is failed; this determines the complete release of the element on the upper mesh near the crack tip. The element on the lower mesh moves downward, too, but being still held in part, the movement is small. The next advance in the crack length (Fig. 3d) frees the lower element and only partially the upper. Figure 3e shows the effect of the releasing yet another interval. Similarly, when all of the intervals are failed, the FE model behaves as though the first interface element is not present. Then, the next interface element starts failing. In this example, intervals whose length is half of the smaller FE extension have been used. Dividing the interface element into more intervals or reducing its length would obviously improve the accuracy of the model.

The present model is intended for pure mode 1 or 2 crack-tip deformation. The method can readily be extended to mixed-mode delamination through a careful consideration of the mode mix conditions.

Energetic Approach for Obtaining Correct Distribution of Stress near the Crack Tip

Initial numerical testing on the developed damage technique produced very good results for mode 2 delamination, but prediction of mode 1 behavior was sometimes inaccurate. To identify the causes of the problem, linear elastic fracture mechanics prediction of the stress distribution near the crack tip was compared to the one obtained with the interface model.[22–25]

Geometry and loads for the mode 1 case are shown in Fig. 4a, whereas original and deformed meshes of the FE model are shown in Fig. 4b. The material has Young's modulus 1 MPa, and the thickness is 1 mm. Two meshes compose the FE model; they are joined

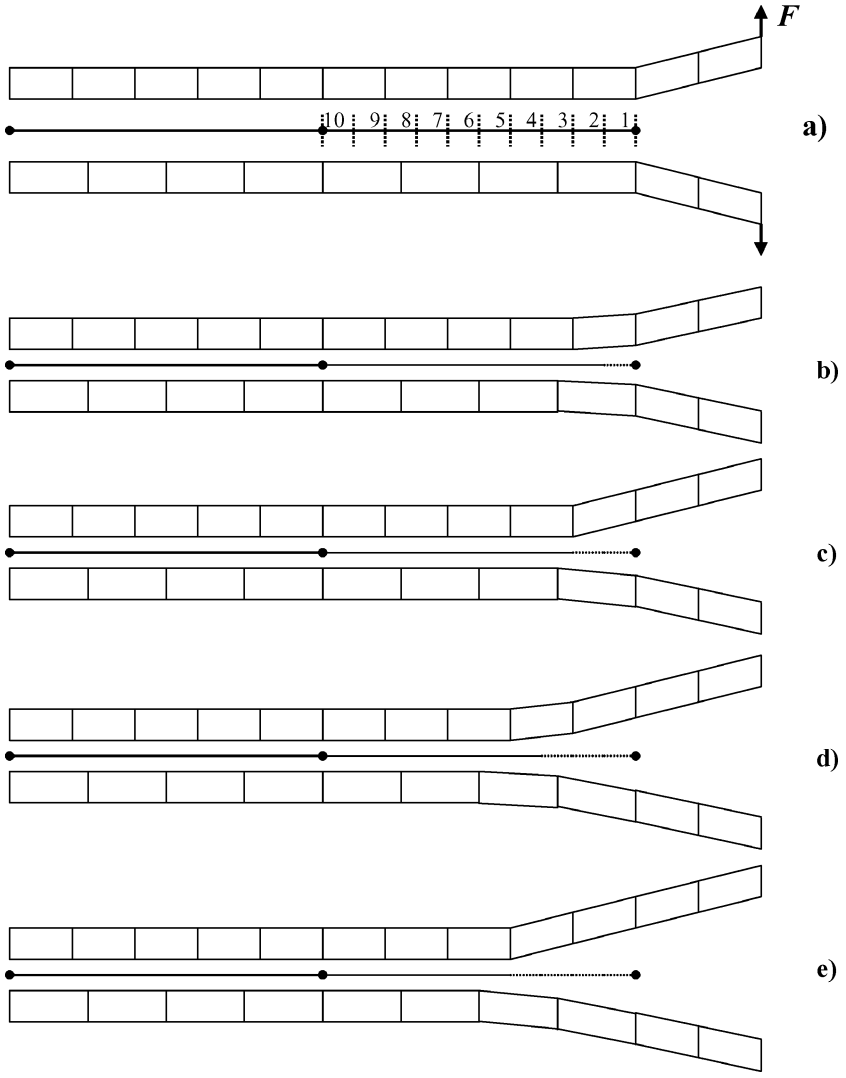

Fig. 3 Division of the interface element in intervals.

by interface elements along the expected crack growth path. Each interface element (1 mm long) connects four FEs (0.5 mm long): two on the bottom mesh and two on the top. The two meshes are compatible in this case. Normal stress σ_{yy} is obtained along the interface, taking advantage of the peculiar abilities of the interface element in recovering the forces at the interface.

Figure 5 shows the stress distribution along the entire interface, whereas Fig. 6 plots σ_{yy} along the first two interface elements next to the crack tip. Stress values in Figs. 5 and 6 are reported in a discrete form; they are averaged at the center of the 10 intervals in which the interface element is divided.

The fracture mechanics solution for an isotropic linear elastic body is computed according to the following equations:

$$\sigma_{yy}(K,\theta,r) = \frac{K}{\sqrt{2\pi r}}\left[1 + \sin\left(\frac{\theta}{2}\right)\sin\left(\frac{3\theta}{2}\right)\right]\cos\left(\frac{\theta}{2}\right) \tag{14}$$

$$K = f1(2.5, 10)\cdot\sqrt{(2.5\pi)} \tag{15}$$

$$f1(a,b) = 1.122 - 0.231\left(\frac{a}{b}\right) + 10.550\left(\frac{a}{b}\right)^2 - 27.710\left(\frac{a}{b}\right)^3 + 30.382\left(\frac{a}{b}\right)^4 \tag{16}$$

$$\sigma_i(x_1,x_2) = \frac{\int_{x_1}^{x_2}\sigma_{yy}(K,0,r)\,\mathrm{d}r}{x_2 - x_1} \tag{17}$$

where σ_i is the average value of the stress σ_{yy} inside one interval. Equation (14) is strictly valid for isotropic materials. It is used here only to obtain an improved distribution of the stresses near the crack tip, as will be described. If known, then the exact order of the singularity for adjacent orthotropic plies could be used instead of the distribution assumed here.

If we observe the stress distribution predicted by the interface element model, it is easy to notice an abnormal behavior along the first interface element. This behavior can be explained if we remember that in the adopted penalty method the continuity constraint is not enforced exactly. Instead, the integral of the square of the relative displacement must be a very small number. The inaccuracy observed in Fig. 6 occurs only when very strong gradient of stresses are present at the interface.

Mesh refinement would improve and eventually correct the results, but it is preferred that the model behave correctly for every possible discretization of the domain especially because the accuracy of the delamination model strongly depends on a precise calculation of the stress and displacement distributions at the crack tip.

The approach for overcoming the problem came from energetic consideration: It is possible to relate the fracture mechanics stress distribution to the interface model solution by imposing that they must contribute equally to the total potential energy of the system. The energy associated with the continuity constraint imposed by the penalty parameter can be expressed also in the following form:

$$E(\delta) = \frac{1}{2}\gamma\int_0^L \delta^2\,\mathrm{d}s \tag{18}$$

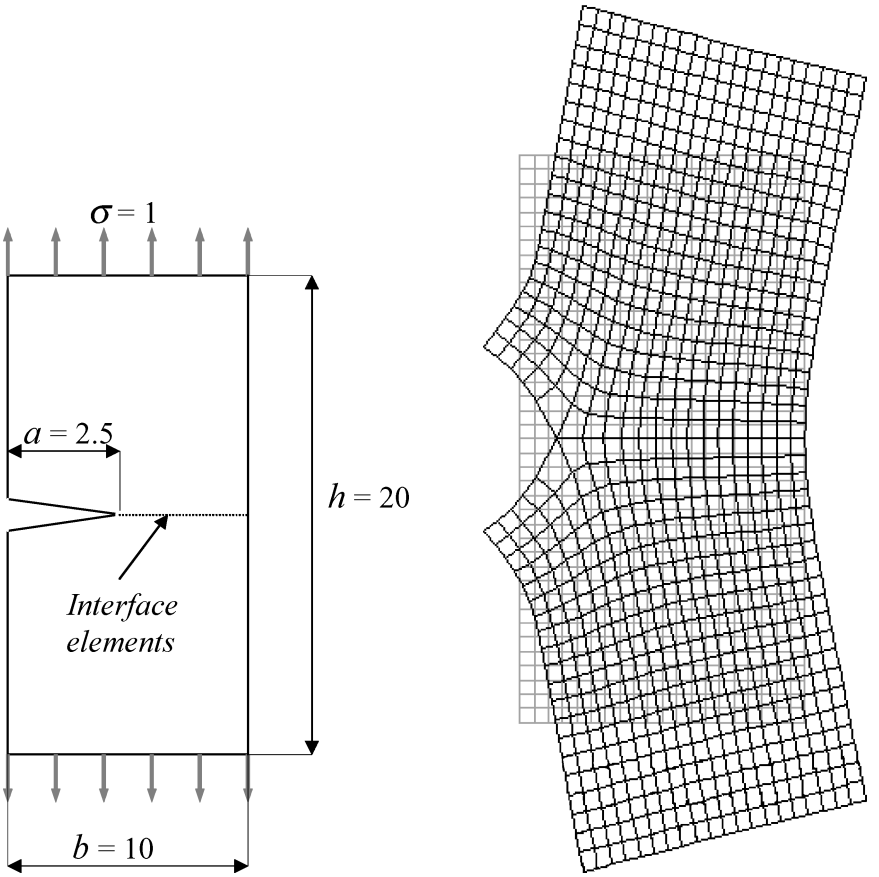

Fig. 4 Fracture mechanics model.

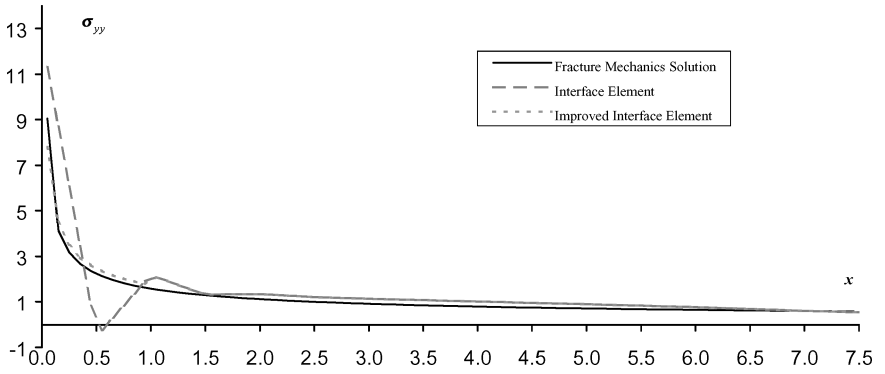

Fig. 5 Normal stress distribution along the entire interface.

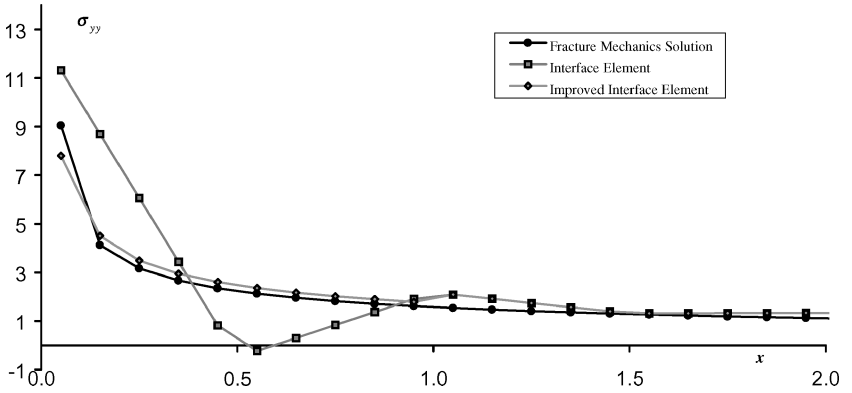

Fig. 6 Normal stress distribution along the first two interface elements next to the crack tip.

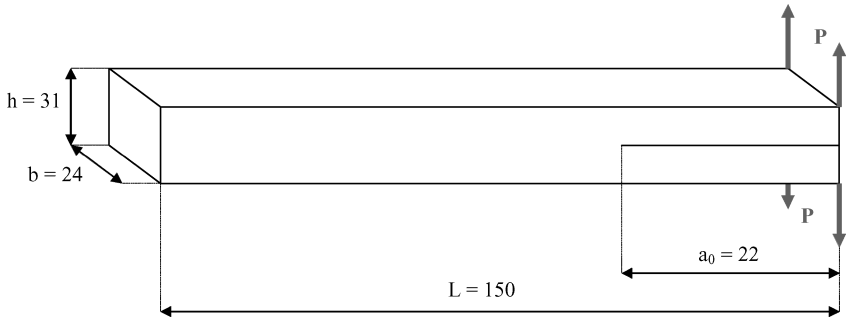

Fig. 7 Geometry and boundary conditions for the DCB test specimen.

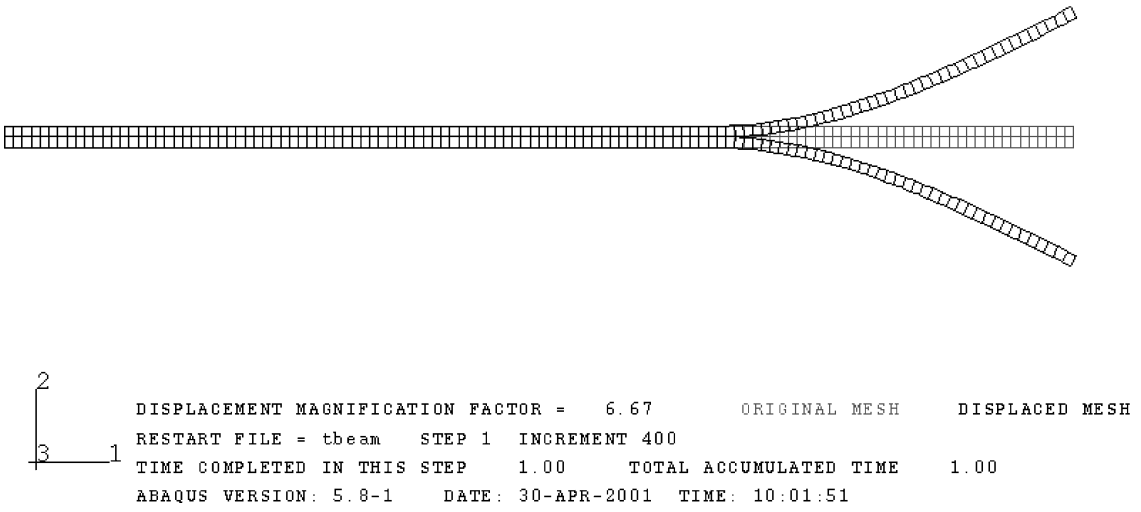

Fig. 8 Original and deformed (5-mm opening) models of the DCB test specimen using a 120 × 2 mesh.

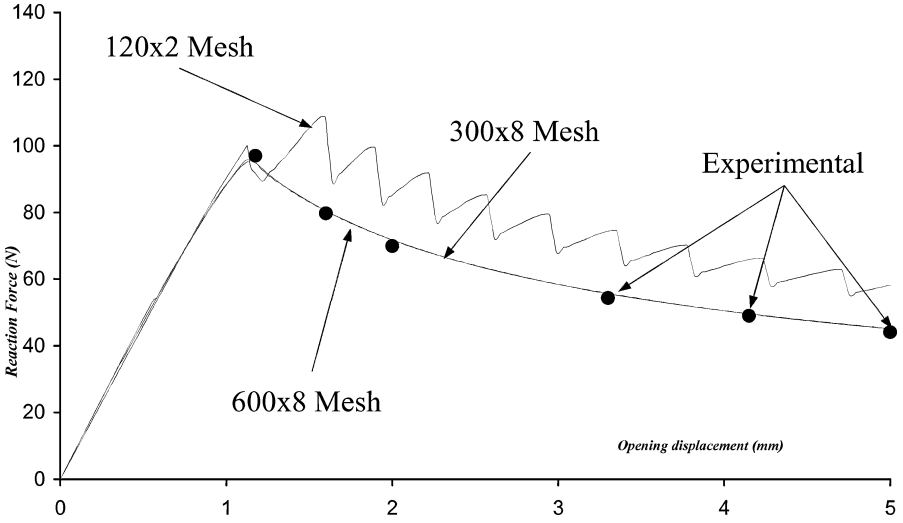

Fig. 9 Force vs displacement results of experimental and numerical DCB test.

where δ is the relative displacement of the connected interfaces and is a function of the position along the interface $\delta = [u_2(s) - u_1(s)] = \delta(s)$. Fracture mechanics predicts, both for mode 1 and mode 2 opening, the stress to vary near the crack tip according to

$$\sigma = \sigma(r, K, \theta) \tag{19}$$

For a given geometry and load applied to the system, K does not change. Moreover, along the interface $\theta = 0$, it follows that

$$\sigma(r) = C_1/\sqrt{r} \tag{20}$$

for an isotropic material, where r is the distance from the crack tip and C_1 is a constant.

In the penalty interface element approach, the stress at any location is a direct function of the penalty parameter and the relative displacement δ:

$$\sigma(\gamma, \delta) = C_2 \cdot \gamma\delta \tag{21}$$

where C_2 is a constant. Now, we want replace the $\delta(s)$ distribution obtained from the FE model with a new one, $\delta'(s)$, such that

$$E(\delta) = E(\delta') \tag{22}$$

If we choose $\delta'(s)$ to be

$$\delta'(s) = C_3/\sqrt{s} \tag{23}$$

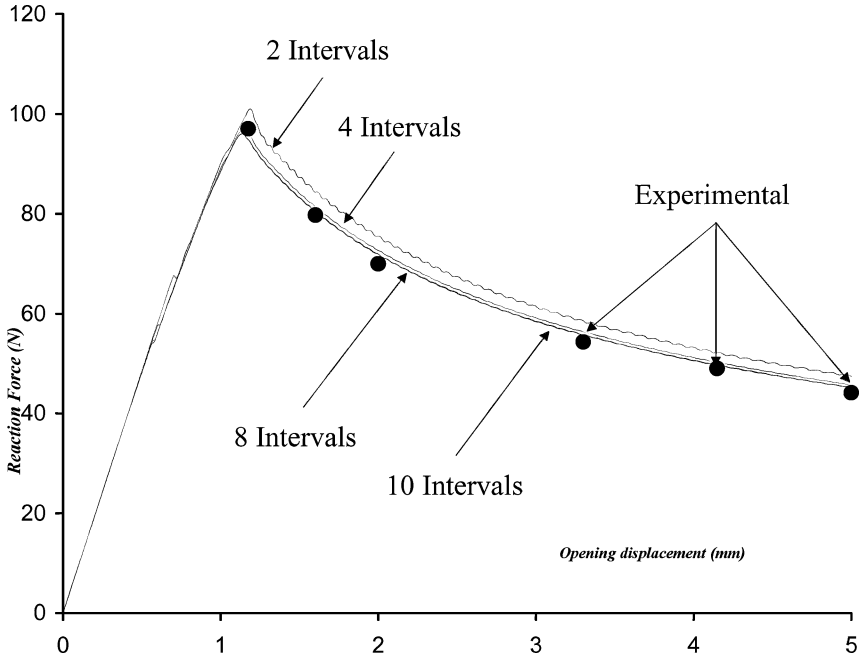

Fig. 10 Force vs displacement results of DCB test; convergence of the solution with intervals number, mesh 300 × 8.

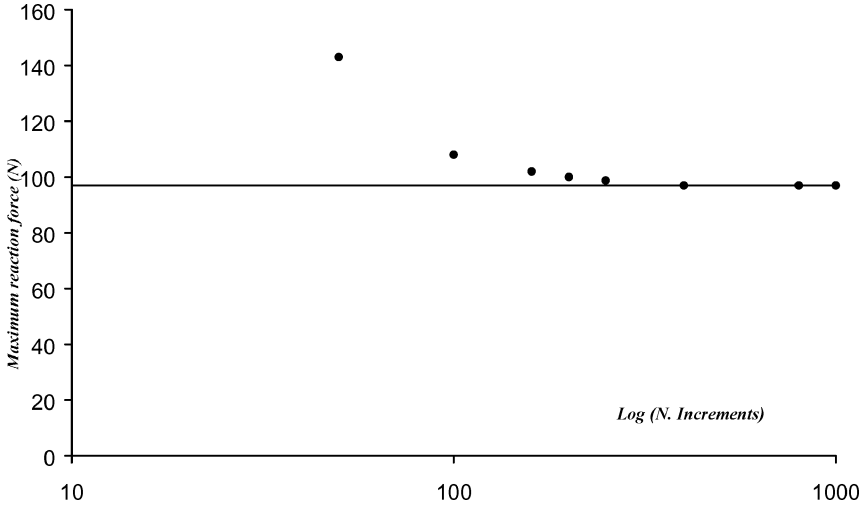

Fig. 11 Convergence of the solution with the number of increments, mesh 300 × 8.

It follows that

$$\sigma(s) = C_4 \big/ \sqrt{s} \tag{24}$$

This means that the stress would vary along the interface according to the fracture mechanics predictions. The constant C_3, in the expression for $\delta'(s)$, is computed by imposing the energetic constraint $E(\delta) = E(\delta')$:

$$E(\delta) = \frac{1}{2}\gamma \int_{s_1}^{s_2} (\delta')^2 \, \mathrm{d}s \tag{25}$$

$$E(\delta) = \frac{1}{2}\gamma \int_{s_1}^{s_2} \frac{C_3^2}{s} \, \mathrm{d}s = \frac{1}{2}\gamma C_3^2 [\ell_n s_2 - \ell_n s_1] \tag{26}$$

$E(\delta)$ is a known quantity that is computed once $\delta(s)$ is obtained from the FE solution. Though the described approach is expressed in terms of energy, the effect is simply to match the integral of the square of the stress to improve the distribution of the predicted stresses in the interface model. The resulting improved stress distribution is plotted in Figs. 5 and 6.

Numerical Results

Double Cantilever Beam Test

The loading, the boundary conditions, and the geometry for the double cantilever beam (DCB) specimen are shown in Fig. 7. The DCB test is recognized as an accurate pure mode 1 test. The properties assumed for the beam material are $E_{11} = 130$ GPa, $E_{22} = E_{33} = 8$ GPa, $G_{12} = 6$ GPa, and $\nu = 0.27$. The properties of the DCB specimen interface are $G_{Ic} = 257$ N/m and $\sigma_t = 20$ MPa.

Three FE models of varying mesh refinement have been used to verify the capabilities of the present approach. In Fig. 8, original and deformed models of the DCB test specimen are shown for the coarsest mesh. Two independent meshes compose the FE models of the upper and lower part of the beam; they are joined by several interface elements. Each interface element connects four FEs: two on the bottom mesh and two on the top. Experimental results used to validate the present delamination approach have been reported by Chen et al.[20] The reaction force as a function of the applied end displacement is shown in Fig. 9. Results from the experiment are compared to analytical results for all of the FE models: mesh 120 × 2, mesh 300 × 8, and mesh 600 × 8.

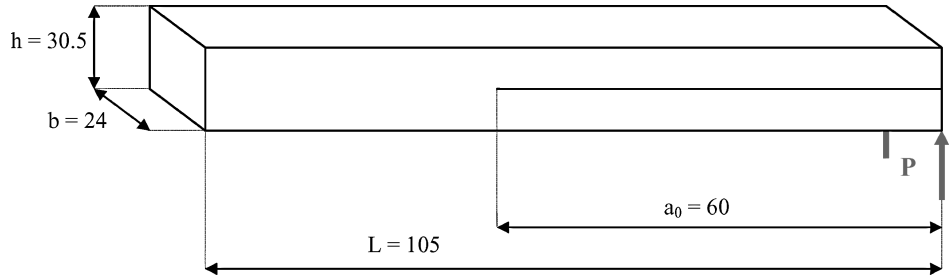

Fig. 12 Geometry and boundary conditions for the ELS test specimen.

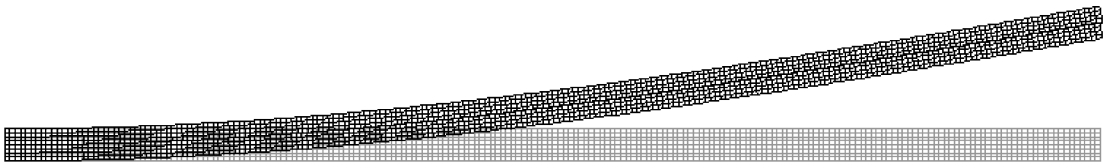

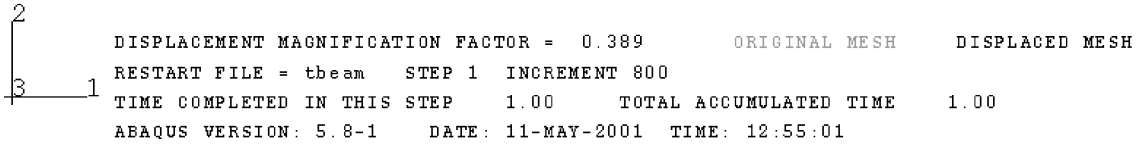

Fig. 13 Original and deformed (30-mm tip displacement) models of the ELS test specimen for a 300 × 8 mesh.

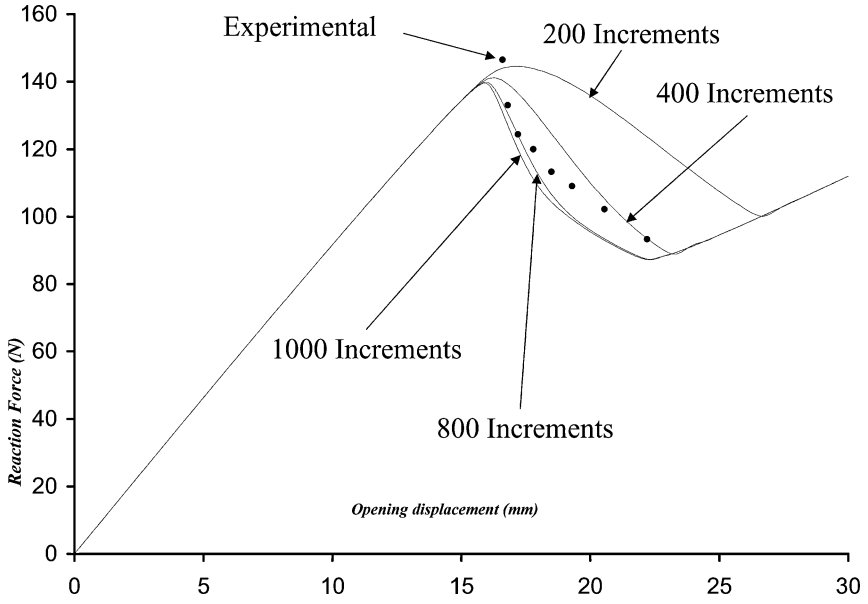

Fig. 14 Force vs displacement results of experimental and analytical ELS test for varying number of loading increments.

Note that the total number of elements in the meshes is indicated; for example, two 120 × 1 meshes joined by interface elements compose the 120 × 2 mesh. The outcomes from 120 × 2 mesh present many local bumps. Mi et al.[17] have analyzed this phenomenon and concluded that coarse meshes can induce these false instabilities. As the mesh is refined, the predicted response agrees very well with that measured experimentally.

As already discussed, the damage technique implemented in our model allows portions of the interface, or intervals, much smaller than the FE length to be released. This allows an improved prediction of the material state in which the crack front is tracked with greater fidelity. In Fig. 10, convergence of the solution with the number of intervals is investigated for the 300 × 8 mesh. Notice that as the number of intervals increases the accuracy of the results increases. Figure 11 shows the model behavior as function of the number of increments for the 300 × 8 mesh. Convergence of the solution to the experimental one is achieved by increasing number of intervals.

End-Loaded Split Beam Test

To characterize the mode 2 delamination shearing mode, the end-loaded split (ELS) specimen is often used. The loading, the boundary conditions, and the geometry for the ELS specimen are shown in Fig. 12.

The properties assumed for the beam material are $E_{11} = 100$ GPa, $E_{22} = E_{33} = 8$ GPa, $G_{12} = 6$ GPa, and $\nu = 0.27$. The properties of the ELS specimen interface are $G_{Ic} = 856$ N/m and $\sigma_t = 48$ MPa.

As in the DCB test specimen models, two meshes compose the FE models of the ELS specimen; they are joined by several interface elements. For the results shown, a 300×8 FE mesh has been utilized.

In Fig. 13, original and deformed models of the ELS test specimen are shown. Experimental results used to validate the present delamination approach have been reported by Chen et al.[20] The reaction force as function of the applied end displacement is shown in Fig. 14. Convergence of the solution as the number of increments increases is demonstrated. These results indicate that the model is reliable and accurate.

Conclusions

A new interface element technology has been presented for predicting crack growth in laminated structures. This interface method is capable of joining and simulating crack growth between independently modeled FE subdomains, for example, composite plies. The interface element approach makes it possible to release subregions of the interface surface whose length is smaller than that of the FEs, thereby allowing for a mesh-independent tracking of the crack front. Results for DCB and ELS specimens indicate that the method is capable of accurately predicting delamination growth.

Acknowledgments

This work was sponsored by NASA Langley Research Center under Grant NAG-1-02061. Partial support was also provided by the State of Michigan Research Excellence Fund. The authors are grateful for the helpful comments of Jonathan Ransom and Carlos Davila.

References

[1]Aminpour, M. A., and Hosapple, K. A., "Finite Element Solutions for Propagating Interface Crack with Singularity Elements," *Engineering Fracture Mechanics*, Vol. 39, No. 3, 1991, pp. 451–468.

[2]Jinping, Z., and Huizu, A., "Stress Analysis Around Holes in Orthotropic Plates by Subregion Mixed Finite Element Method," *Computers and Structures*, Vol. 41, No. 1, 1991, pp. 105–108.

[3]Farhat, C., and Roux, F. X., "A Method of Finite Element Tearing and Interconnecting and Its Parallel Solution Algorithm," *International Journal for Numerical Methods in Engineering*, Vol. 32, 1991, pp. 1205–1227.

[4]Farhat, C., and Gerardin, M., "Using a Reduced Number of Lagrange Multipliers for Assembling Parallel Incomplete Field Finite Element Approximations," *Computer Methods in Applied Mechanics and Engineering*, Vol. 97, 1992, pp. 333–354.

[5]Maday, Y., Mavriplis, C., and Patera, A., "Non-Conforming Mortar Element Methods: Application to Spectral Discretizations," NASA CR-181729, ICASE Rept. 88-59, 1988.

[6]Ransom, J. B., McCleary, S. L., and Aminpour, M. A., "A New Interface Element for Connecting Independently Modeled Substructures," AIAA Paper 93-1503, 1993.

[7]Housner, J. M., Aminpour, M. A., Dávila, C. G., Schiermeier, J. E., Stroud, W. F., Ransom, J. B., and Gillian, R. E., "An Interface Element for Global/Local and Substructuring Analysis," MSC 1995 World Users' Conf. Proceedings, Paper 25, MSC Software Corp., Santa Cruz, CA, May 1995.

[8]Aminpour, M. A., Ransom, J. B., and McCleary, S. L., "A Coupled Analysis Method for Structures with Independently Modeled Finite Element Subdomains," *International Journal for Numerical Methods in Engineering*, Vol. 38, 1995, pp. 3695–3718.

[9]Ransom, J. B., "Interface Technology for Geometrically Nonlinear Analysis of Multiple Connected Subdomains," AIAA Paper 97-1298, 1997.

[10]Aminpour, M. A., and Krishnamurthy, T., "A Two-Dimensional Interface Element for Multi-Domain Analysis of Independently Modeled Three-Dimensional Finite Element Meshes," AIAA Paper 97-1297, 1997.

[11]Aminpour, M. A., Krishnamurthy, T., and Fadale, T. D., "Coupling of Independently Modeled Three-Dimensional Finite Element Meshes with Arbitrary Shape Interface Boundaries," AIAA Paper 98-2060, 1998.

[12]Aminpour, M. A., Pageau, S., and Shin, Y., "An Alternative Method for the Interface Modeling Technology," AIAA Paper 2000-1352, 2000.

[13]Cho, M., and Kim, W. B., "A Coupled Finite Element Analysis of Independently Modeled Substructures by Penalty Frame Method," AIAA Paper 98-2061, 1998.

[14]Schellekens, J. C. J., and De Boerst, R., "A Non-Linear Finite Element Approach for the Analysis of Mode-I Free Edge Delamination in Composites," *International Journal of Solids and Structures*, Vol. 30, No. 9, 1993, pp. 1939–1953.

[15]Lammerant, L., and Verpoest, I., "Modeling of the Interaction Between Matrix Cracks and Delaminations During Impact of Composite Plates," *Composites Science and Technology*, Vol. 56, No. 10, 1996, pp. 1171–1178.

[16]Reedy, E. D., Jr., Mello, F. J., and Guess, T. R., "Modeling the Initiation and Growth of Delaminations in Composite Structures," *Journal of Composite Materials*, Vol. 31, No. 8, 1997, pp. 812–831.

[17]Mi, Y., Crisfield, A., Davies, A. O., and Hellweg, H. B., "Progressive Delamination Using Interface Elements," *Journal of Composite Materials*, Vol. 32, No. 14, 1998, pp. 1246–1272.

[18]Schipperen, J. H. A., and Lingen, F. J., "Validation of Two-Dimensional Calculation of Free-Edge Delamination in Laminated Composites," *Composite Structures*, Vol. 45, 1999, pp. 233–240.

[19]Dakshima Moorthy, C. M., and Reddy, J. N., "Recovery of Interlaminar Stresses and Strain Energy Release Rates in Composite Laminates," *Finite Elements in Analysis and Design*, Vol. 33, 1999, pp. 1–27.

[20]Chen, J., Crisfield, M., Kinloch, A. J., Busso, E. P., Matthews, F. L., and Qiu, Y., "Predicting Progressive Delamination of Composite Materials Specimens via Interface Elements," *Mechanics of Composite Materials and Structures*, Vol. 6, 1999, pp. 301–317.

[21]Davila, C., Camanho, P. P., and de Moura, M. F., "Mixed-Mode Decohesion Elements for Analyses of Progressive Delamination," AIAA Paper 2001-1486, 2001.

[22]Krausz, A. S., and Krausz, K., *Fracture Kinetics and Crack Growth*, Kluwer Academic, Boston, 1988.

[23]Broek, D., *The Practical Use of Fracture Mechanics*, Kluwer Academic, Boston, 1989.

[24]Aliabadi, M. H., and Rooke, D. P., *Numerical Fracture Mechanics*, Kluwer Academic, Boston, 1991.

[25]Luxmoore, R., and Owen, D. R., "Numerical Methods in Fracture Mechanics," *Proceedings of the First International Conference on Numerical Methods in Fracture Mechanics*, Quadrant, Swansea, Wales, U.K., 1978.

B. V. Sankar
Associate Editor